Matrix Isolation Infrared Spectroscopic and Density Functional Theory Studies on the Reactions of Yttrium and Lanthanum Hydrides with Dinitrogen

Yun-Lei Teng and Qiang Xu*

National Institute of Advanced Industrial Science and Technology (AIST), Ikeda, Osaka 563-8577, Japan, and Graduate School of Engineering, Kobe University, Nada Ku, Kobe, Hyogo 657-8501, Japan

Received: February 23, 2008; Revised Manuscript Received: June 5, 2008

Laser-ablated yttrium and lanthanum hydrides have been codeposited at 4 K with dinitrogen in excess argon. Products, $HY(N_2)$, HYNN, H_2YNN, HLaNN, and H_2LaNN, have been formed in the present experiments and characterized by using infrared spectroscopy on the basis of the results of the isotopic shifts, mixed isotopic splitting patterns, stepwise annealing, and comparison with theoretical predictions. Density functional theory calculations have been performed on these molecules. The agreement between the experimental and calculated vibrational frequencies, relative absorption intensities, and isotopic shifts supports the identification of these molecules from the matrix infrared spectra. Plausible reaction mechanisms have been proposed for the formation of these molecules.

Introduction

The bonding of dinitrogen with transition metals is of great interest from both academic and industrial viewpoints because binding of dinitrogen to transition metal centers may lead to the cleavage of the strong N−N bond as in the catalytic synthesis of ammonia.[1−3] The long-standing goal of elucidating mechanisms of the reactions involving dinitrogen has motivated numerous experimental and theoretical investigations of the interactions between metals and dinitrogen.[4−11] For example, the reactions of laser-ablated yttrium and lanthanum with dinitrogen have been extensively studied, and various Y and La nitrides and dinitrogen complexes have been characterized.[11a,b]

Metal hydrides are important as hydrogen storage materials for fuel cells.[12a] For instance, the $LaNi_5$ alloy has been found to reversibly absorb/desorb hydrogen.[12b,c] The reactions of laser-ablated Sc, Y, and La with molecular hydrogen in excess argon have been reported, and the products MH, MH_2^+, MH_2, and MH_4^- (M = Sc, Y, and La) have been characterized by infrared spectroscopy.[13] Recently, we reported the reactions of laser-ablated yttrium and lanthanum hydrides with carbon monoxide, and the products HYCO, $(HY)_2CO$, HLaCO, $HLa(CO)_2$ and H_2LaCO have been formed and characterized by using infrared spectroscopy.[14] On the other hand, there are no reports on the reactions of metal hydride with dinitrogen, although a number of important metal-catalyzed reactions using nitrogen and hydrogen, such as ammonia synthesis, involve metal-dinitrogen-hydride species as the reaction intermediates; such metal-dinitrogen-hydride species may play an important role in the reaction process.

Recent studies have shown that with the aid of isotopic substitution techniques, matrix isolation infrared spectroscopy combined with quantum chemical calculation is very powerful for investigating the structure and bonding of novel species.[15] To understand the formation of dinitrogen-hydride species of yttrium and lanthanum, the reactions of laser-ablated yttrium and lanthanum hydrides with dinitrogen in a solid-argon matrix have been performed. IR spectroscopy and theoretical calculations provide evidence for the formation of products $HY(N_2)$, HYNN, H_2YNN, HLaNN, and H_2LaNN.

* Author to whom correspondence should be addressed. E-mail: q.xu@aist.go.jp.

Experimental and Theoretical Methods

The experiments for laser-ablation and matrix-isolation infrared spectroscopy are similar to those previously reported.[16] Briefly, the Nd:YAG laser fundamental (1064 nm, 10 Hz repetition rate with 10 ns pulse width) was focused on the rotating YH_2 (>99.9%, High Purity Chemicals) and LaH_x (>99%, High Purity Chemicals) targets. The laser-ablated species were codeposited with N_2 (99.95%) in excess argon onto a CsI window cooled normally to 4 K by means of a closed-cycle helium refrigerator (V24SC6LSCP, Daikin Industries). Typically, a 5−30 mJ/pulse laser power was used. Isotopic substituted $^{15}N_2$ (99.8%) and $^{14}N_2 + {}^{15}N_2$ and high-frequency-discharging scrambled $^{14}N_2 + 2{}^{14}N^{15}N + {}^{15}N_2$ mixtures were used in different experiments. In general, matrix samples were deposited for 30−60 min with a typical rate of 2−4 mmol per hour. After sample deposition, IR spectra were recorded on a BIO-RAD FTS-6000e spectrometer at 0.5 cm^{-1} resolution by using a liquid nitrogen cooled HgCdTe (MCT) detector for the spectral range of 5000−400 cm^{-1}. Samples were annealed at different temperatures.

Quantum chemical calculations were performed to predict the structures and vibrational frequencies of the observed reaction products by using the Gaussian 03 program.[17] The spin restricted and unrestricted BP86 and B3PW91 density functional methods were utilized.[18] The 6-311++G(d, p) basis set was used for H and N atoms, and SDD was used for Y and La atoms.[19,20] Geometries were fully optimized, and vibrational frequencies were calculated with analytical second derivatives.

Results and Discussion

Experiments have been done with N_2 concentrations ranging from 0.05 to 0.5% in excess argon. Typical infrared spectra for the reactions of laser-ablated YH_2 and LaH_x with N_2 in excess argon in the selected regions are illustrated in Figures 1−4, and the absorption bands are listed in Table 1. The stepwise

10.1021/jp8016024 CCC: $40.75
Published on Web 07/30/2008

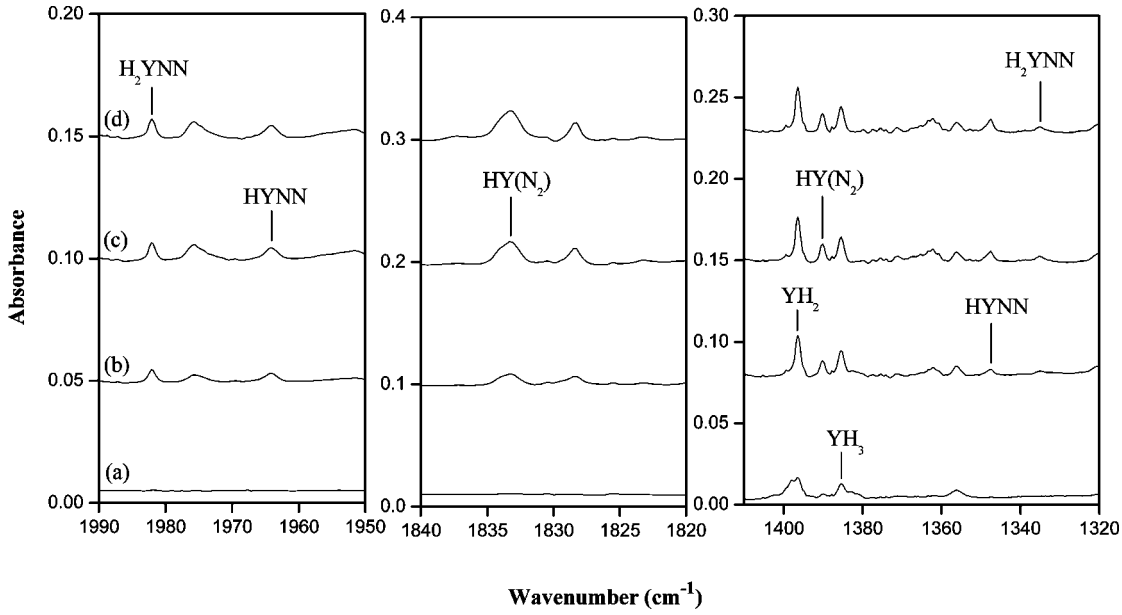

Figure 1. Infrared spectra in the 1990−1950, 1840−1820, and 1410−1320 cm^{-1} regions from codeposition of laser-ablated yttrium hydride with 0.2% N_2 in argon (a) 60 min sample deposition at 4 K, (b) after annealing to 25 K, (c) after annealing to 30 K, and (d) after annealing to 35 K.

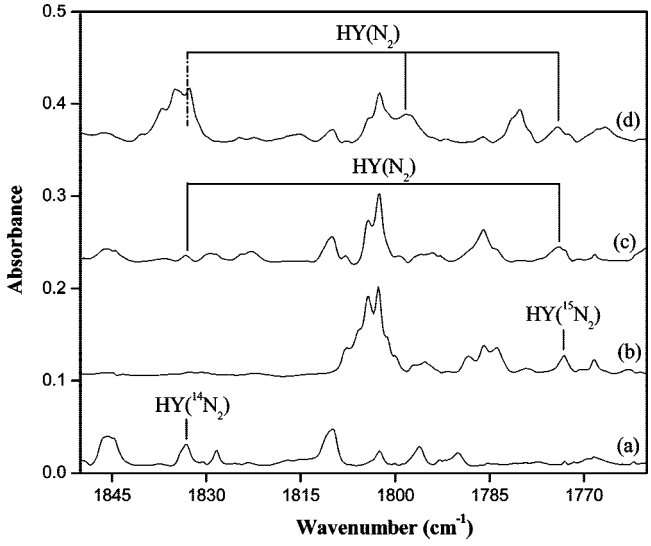

Figure 2. Infrared spectra in the 1850−1760 cm^{-1} region from codeposition of laser-ablated yttrium hydride with N_2 in argon after annealing to 35 K. (a) 0.2% $^{14}N_2$, (b) 0.2% $^{15}N_2$, (c) 0.2% $^{14}N_2$ + 0.2% $^{15}N_2$, and (d) 0.2% $^{14}N_2$ + 0.4% $^{14}N\,^{15}N$ + 0.2% $^{15}N_2$.

annealing behavior of these product absorptions are also shown in the figures and will be discussed below.

Quantum chemical calculations have been carried out for the possible isomers and electronic states of the potential product molecules. Figure 5 shows the optimized structures and electronic ground states. Table 2 reports a comparison of the observed and calculated IR frequencies and isotopic frequency ratios of the reaction products. Calculated vibrational frequencies and intensities of the potential products are listed in Table 3.

$HY(N_2)$. Laser ablation of an YH_2 target gives rise to a strong IR absorption at 1470.5 cm^{-1} due to YH, absorptions at 1458.6 and 1396.4 cm^{-1} due to YH_2, and absorption at 1385.4 cm^{-1} due to YH_3.[13] In addition to the absorptions due to yttrium nitrides and dinitrogen complexes observed in the experiments of laser ablation of Y with N_2[11a,b] and the absorptions due to the yttrium hydrides observed in the experiments of laser ablation of YH_2, new absorptions at 1982.1, 1964.2, 1833.2, 1390.1, 1347.6, and 1335.1 cm^{-1} are observed in the experiments of laser ablation of YH_2 with N_2. The absorptions at 1833.2 and 1390.1 cm^{-1} appear on sample annealing to 25 K and further increase on annealing to 30 and 35 K (Table 1 and Figure 1). The 1833.2 cm^{-1} band shifts to 1773.0 cm^{-1} with $^{15}N_2$, exhibiting isotopic frequency ratios ($^{14}N/^{15}N$ = 1.0340) characteristic of N−N stretching vibration. As shown in Figure 2, the mixed $^{14}N_2$ + $^{15}N_2$ isotopic spectra only provide the sum of pure isotopic bands, which indicates that only one N_2 subunit is involved in this mode. In the experiment with the 0.2% $^{14}N_2$ + 0.4% $^{14}N^{15}N$ + 0.2% $^{15}N_2$, three absorptions at 1833.2, 1798.1, and 1774.1 cm^{-1} are produced (Figure 2), which implies that a side-bonded N_2 subunit is involved. The absorptions at 1833.2 cm^{-1} (A = absorbance = 0.035) and 1390.1 cm^{-1} (A = 0.015) can be grouped together to one species on the basis of the growth/decay characteristics as a function of changes of experimental conditions. The position of the 1390.1 cm^{-1} band indicates a Y−H stretching vibration. Doping with CCl_4 has no effect on the two bands, which suggests that the product is neutral. The 1833.2 and 1390.1 cm^{-1} bands are therefore assigned to the N−N and Y−H stretching vibrations of the neutral $HY(N_2)$ molecule, respectively.

BP86 calculations predict that $HY(N_2)$ has an ^3A ground-state with C_1 symmetry (Figure 5), which is 4.3 and 68.8 kcal/mol lower in energy than the singlet and quintet ones, respectively. The molecule is predicted to have a $(core)(a)^2(a)^1(a)^1(a)^0$ configuration. The calculated N−N distance in $HY(N_2)$ is 1.172 Å, lengthened by 0.064 Å compared with that in N_2. As shown in Table 2, the calculated N−N stretching and Y−H stretching vibrations for $HY(N_2)$ are 1833.6 and 1462.9 cm^{-1}, respectively, in agreement with the experimental observations (1833.2 and 1390.1 cm^{-1}). As the two N atoms are inequivalent, four absorptions at 1833.6, 1803.0, 1802.8, and 1771.7 cm^{-1} are expected for the experiment with the $^{14}N_2$ + $^{14}N^{15}N$ + $^{15}N_2$ according to our DFT calculations. The two intermediate $^{14}N-^{15}N$ bands are so near that they may overlap each other, which is consistent with our observations.

HYNN. The absorptions at 1964.2 cm^{-1} (A = 0.01) and 1347.6 cm^{-1} (A = 0.007) appears on annealing to 25 K and

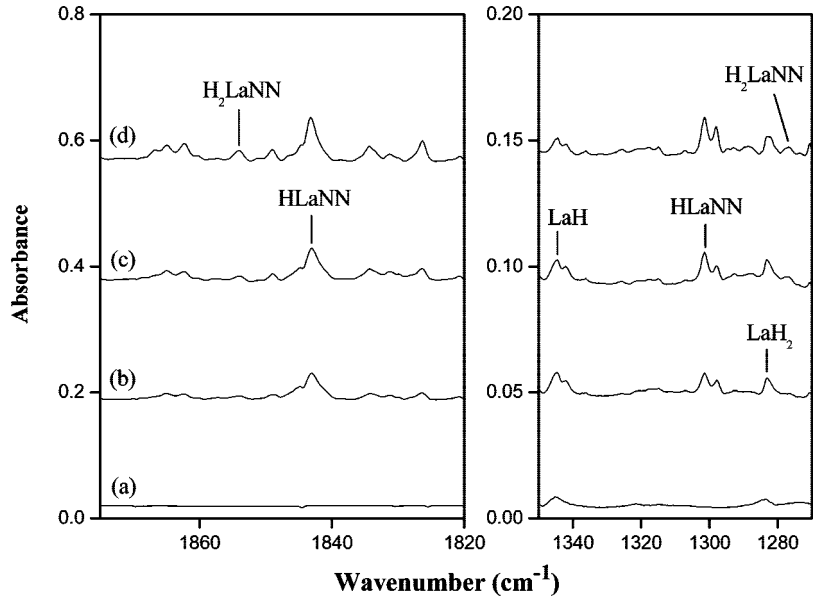

Figure 3. Infrared spectra in the 1875−1820 and 1350−1270 cm^{-1} regions from codeposition of laser-ablated lanthanum hydride with 0.1% N_2 in argon (a) 45 min sample deposition at 4 K, (b) after annealing to 25 K, (c) after annealing to 30 K, and (d) after annealing to 35 K.

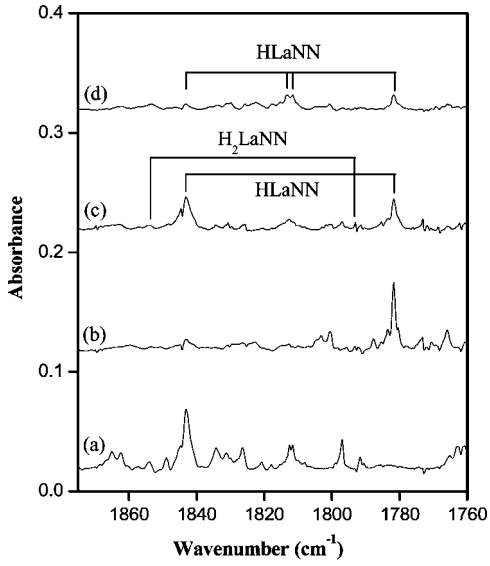

Figure 4. Infrared spectra in the 1875−1760 cm^{-1} region from codeposition of laser-ablated lanthanum hydride with N_2 in argon after annealing to 30 K. (a) 0.1% $^{14}N_2$, (b) 0.1% $^{15}N_2$, (c) 0.1% $^{14}N_2$ + 0.1% $^{15}N_2$, and (d) 0.1% $^{14}N_2$ + 0.2% $^{14}N\,^{15}N$ + 0.1% $^{15}N_2$.

visibly increases on further annealing to 30 and 35 K (Table 1 and Figure 1). The 1964.2 cm^{-1} band shifts to 1899.1 cm^{-1} with $^{15}N_2$, exhibiting isotopic frequency ratio ($^{14}N/^{15}N = 1.0343$) characteristic of N−N stretching vibration. The mixed $^{14}N_2$ and $^{15}N_2$ isotopic spectra only provide the sum of pure isotopic bands, which indicates that only one N_2 subunit is involved in this mode. The position of the 1964.2 cm^{-1} band indicates that an end-bonded N_2 subunit is involved. The absorption at 1347.6 cm^{-1} exhibits the same annealing behavior as that of the 1964.2 cm^{-1} band, suggesting that the two absorptions are due to the different modes of the same molecule. The position of the 1347.6 cm^{-1} band indicates a Y−H stretching vibration. Doping with CCl_4 has no effect on the two bands, which suggests that the product is neutral. The 1964.2 and 1347.6 cm^{-1} bands are therefore assigned to the N−N and Y−H stretching vibrations of the neutral HYNN molecule, respectively.

The present DFT calculations lend support for the assignment of HYNN. The HYNN molecule is predicted to have an $^3A''$ electronic ground state with C_s symmetry, which is 1.8 kcal/mol lower in energy than that of the HY(N_2) isomer (Figure 5). The Y−H and N−N bond lengths of ground-state HYNN are calculated to be 1.967 and 1.150 Å, respectively, which are 0.046 and 0.042 Å longer than those of YH and N_2 calculated at the same level. The HYNN molecule can be viewed as being formed by the interaction of the HY fragment and N_2 fragment. The present DFT calculations predict a triplet ground state for HYNN with a (core)$(a')^1(a'')^1(a')^0$ configuration, which correlates to the $^3\Sigma^+$ excited-state HY with the $(1\sigma)^2(2\sigma)^2(1\pi)^4(3\sigma)^2(4\sigma)^1(1\delta)^1(2\pi)^0$ configuration. The open-shell $(a')^1(a'')^1(a')^0$ configuration of HYNN triplet was somewhat surprising because the HY molecule preferred a $^1\Sigma^+$ singlet with a (core)$(1\sigma)^2(1\pi)^4(2\sigma)^2(3\sigma)^2(4\sigma)^2(1\delta)^0$ configuration, and the $^3\Sigma^+$ triplet HY was predicted to lie 10.2 kcal/mol higher in energy than the $^1\Sigma^+$ state. In a similar fashion, the $(NN)_2CrO_2$, $(CO)_2CrO_2$, and $(H_2)_2CrO_2$ molecules that were predicted to have singlet ground states correlated to the excited state $^1A_1$ CrO_2.[9a,21] The interactions are dominated by the synergic donations of filled $3\sigma_g$ orbital of N_2 into the empty 2π acceptor orbital of HY and the back-donation of the δ electrons of HY to the π_g antibonding orbital of N_2. The empty 2π molecule orbital of $^3\Sigma^+$ HY is primarily a nonbonding hydrid of the Y 5s and 4d orbitals. The singly occupied 1δ molecule orbital of $^3\Sigma^+$ HY is largely the Y 4d orbital that is mainly nonbonding. NBO population analysis shows that N_2 subunit transfers about 0.049 e to the HY moiety, whereas there is about 0.009 e back-donation from HY to the N_2 subunit. The N−N and Y−H stretching vibrations for HYNN are calculated at 1925.5 and 1444.1 cm^{-1} (Tables 2 and 3), respectively.

H_2YNN. The absorptions at 1982.1 cm^{-1} ($A = 0.009$) and 1335.1 cm^{-1} ($A = 0.006$) appear on sample annealing to 25 K and further increase on annealing to 30 and 35 K (Table 1 and Figure 1). The 1982.1 cm^{-1} band shifts to 1916.7 cm^{-1} with $^{15}N_2$, exhibiting isotopic frequency ratios ($^{14}N/^{15}N = 1.0341$) characteristic of N−N stretching vibration. The mixed $^{14}N_2$ + $^{15}N_2$ isotopic spectra only provide the sum of pure isotopic bands, which indicates that only one N_2 subunit is involved in this mode. The position of 1982.1 cm^{-1} band indicates that an end-bonded N_2 subunit is involved. The absorptions at 1982.1 and 1335.1 cm^{-1} can be grouped together to one species on the

TABLE 1: Infrared Absorptions (cm^{-1}) from Co-Deposition of Laser-Ablated YH_2 and LaH_x with N_2 in Excess Argon at 4 K

$^{14}N_2$	$^{15}N_2$	$^{14}N_2 + {}^{15}N_2$	$^{14}N_2 + {}^{14}N^{15}N + {}^{15}N_2$	$^{14}N/^{15}N$	assignment (mode)[a]
1982.1	1916.7	1982.4, 1916.6		1.0341	H_2YNN N−N str.
1964.2	1899.1	1964.3, 1899.1		1.0343	HYNN N−N str.
1833.2	1773.0	1833.2, 1773.9	1833.2, 1798.1, 1774.1	1.0340	$HY(N_2)$ N−N str.
1390.1	1390.1	1390.0	1390.0		$HY(N_2)$ Y−H str.
1347.6	1347.9	1347.9	1348.0		HYNN Y−H str.
1335.1	1335.0	1335.1	1335.0		H_2YNN as Y−H str.
1854.1	1793.3	1853.9, 1793.1		1.0339	H_2LaNN N−N str.
1843.1	1781.8	1843.1, 1781.8	1843.2, 1813.3, 1811.6, 1781.8	1.0344	HLaNN N−N str.
1301.5	1301.2	1301.3	1301.4		HLaNN La−H str.
1276.7	1276.7	1276.5	1276.3		H_2LaNN as La−H str.

[a] as, antisymmetric; str., stretching mode.

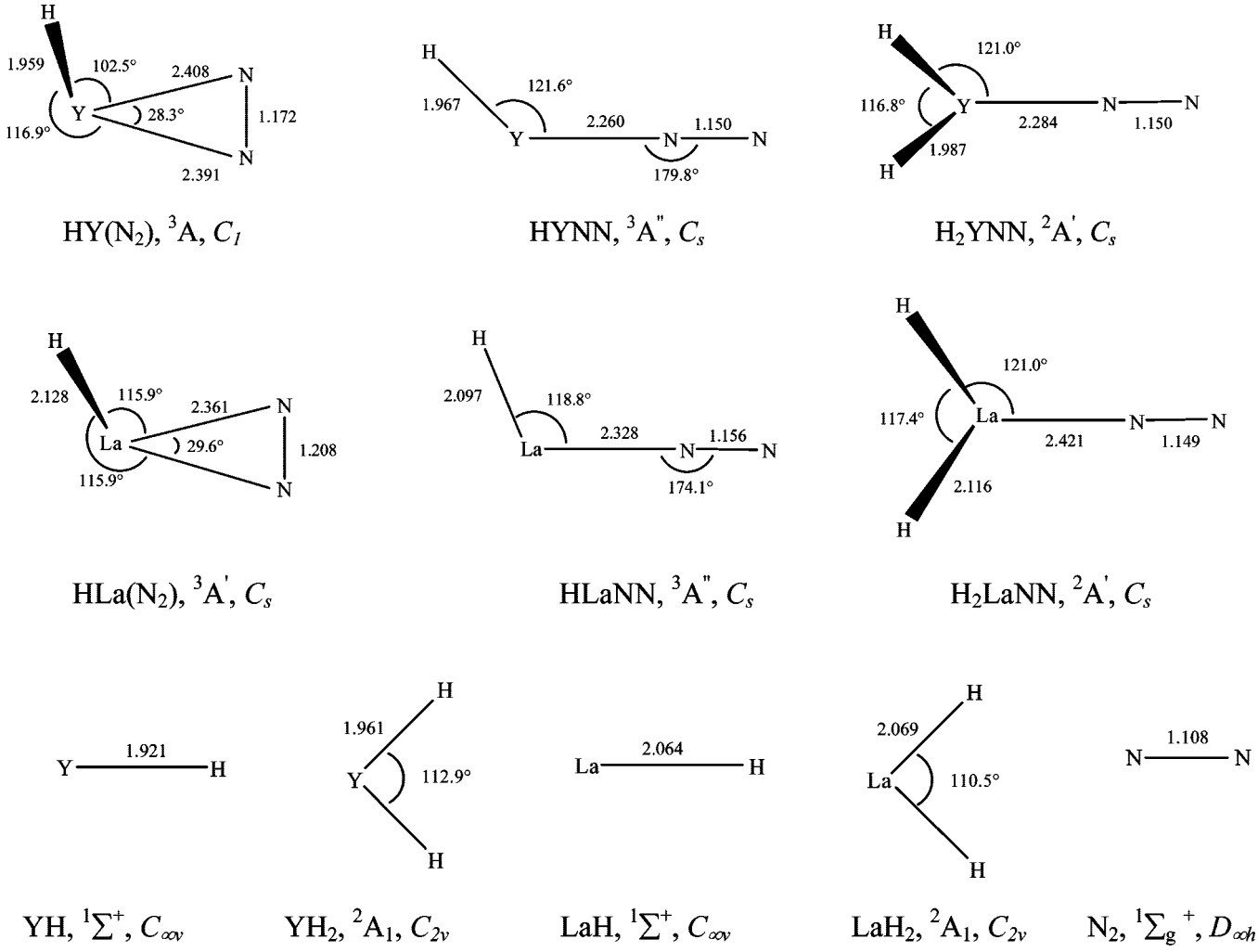

Figure 5. Optimized structures (bond length in angstrom, bond angle in degree), electronic ground states, and point groups of the possible products and isomers calculated at the BP86/6-311++G(d, p)-SDD level (only LaH is calculated by using the B3PW91 method).

basis of the growth/decay characteristics as a function of changes of experimental conditions. The position of the 1335.1 cm^{-1} band indicates a Y−H stretching vibration. Doping with CCl_4 has no effect on the two bands, which suggests that the product is neutral. The 1982.1 and 1335.1 cm^{-1} bands are therefore assigned to the N−N and Y−H stretching vibrations of the neutral H_2YNN molecule, respectively.

BP86 calculations predict that H_2YNN has a $^2A'$ ground state with C_s symmetry (Figure 5). As shown in Table 2, the calculated N−N stretching and antisymmetric Y−H stretching vibrations for H_2YNN are 1951.2 and 1417.2 cm^{-1}, respectively. DFT calculations also predict a symmetric Y−H stretching vibrational frequency at 1452.6 cm^{-1}, which is unfortunately overlapped by other absorptions in the experiment.

Laser ablation of an YH_2 target produces YH_3 molecules. However, no evidence is found for H_3YNN complexes in the present experiments. DFT calculations are performed on the H_3YNN molecule, and no stable structure is found, which is in accord to the experimental observations.

HLaNN. Intense IR absorptions due to LaH (1345.2 cm^{-1}), LaH_2 (1282.9 and 1221.1 cm^{-1}), and LaH_3 (1263.9 cm^{-1}) are observed in the experiment of laser ablation of a LaH_x target, for which the IR absorptions are in agreement with the previous reported values.[13] In addition to the absorptions due to lantha-

TABLE 2: Comparison of Observed and Calculated IR Frequencies (cm^{-1}) and Isotopic Frequency Ratios of the Reaction Products

	freq		$^{14}N/^{15}N$	
mode[a]	obsd	calcd	obsd	calcd
$HY(N_2)$				
N−N str.	1833.2	1833.6	1.0340	1.0349
Y−H str.	1390.1	1462.9		
HYNN				
N−N str.	1964.2	1925.5	1.0343	1.0349
Y−H str.	1347.6	1444.1		
H_2YNN				
N−N str.	1982.1	1951.2	1.0341	1.0350
as Y−H str.	1335.1	1417.2		
HLaNN				
N−N str.	1843.1	1834.5	1.0344	1.0349
La−H str.	1301.5	1341.5		
H_2LaNN				
N−N str.	1854.1	1943.9	1.0339	1.0350
as La−H str.	1276.7	1305.2		

[a] as = antisymmetric, str. = stretching mode.

TABLE 3: Ground Electronic States, Point Groups, Vibrational Frequencies (cm^{-1}), and Intensities (km/mol) of the Reaction Products and Isomers Calculated at the BP86/6-311++G(d, p)-SDD level

species	elec state	point group	frequency (intensity, mode)
$HY(N_2)$	^3A	C_1	1833.6 (600, A), 1462.9 (341, A)
HYNN	$^3A''$	C_s	1925.5 (933, A′), 1444.1 (406, A′)
H_2YNN	$^2A'$	C_s	1951.2 (599, A′), 1452.6 (462, A′), 1417.2 (714, A″), 560.0 (118, A′)
$HLa(N_2)$	$^3A'$	C_s	1603.5 (653, A′), 1320.9 (617, A′), 710.9 (798, A″)
HLaNN	$^3A''$	C_s	1834.5 (1725, A′), 1341.5 (567, A′)
H_2LaNN	$^2A'$	C_s	1943.9 (685, A′), 1340.7 (574, A′), 1305.2 (1021, A″), 545.4 (203, A′)

num nitrides and dinitrogen complexes observed in the experiments of laser ablation of La with N_2[11a,b] and the lanthanum hydrides observed in the experiments of laser ablation of LaH_x, new absorptions at 1854.1, 1843.1, 1301.5, and 1276.7 cm^{-1} are observed in the experiments of laser ablation of LaH_x with N_2. The absorption at 1843.1 cm^{-1} ($A = 0.179$) appears on annealing to 25 K and visibly increases on further annealing to 30 and 35 K (Table 1 and Figure 3). The 1843.1 cm^{-1} band shifts to 1781.8 cm^{-1} with $^{15}N_2$, exhibiting isotopic frequency ratio ($^{14}N/^{15}N = 1.0344$) characteristic of N−N stretching vibration. The mixed $^{14}N_2$ and $^{15}N_2$ isotopic spectra only provide the sum of pure isotopic bands (Figure 4), which indicates that only one N_2 subunit is involved in this mode. In the experiment with the 0.1% $^{14}N_2$ + 0.2% $^{14}N^{15}N$ + 0.1% $^{15}N_2$, four absorptions at 1843.2, 1813.3, 1811.6, and 1781.8 cm^{-1} with approximately 1:1:1:1 relative intensities are produced (Figure 4), which implies that the two N atoms are inequivalent. The absorption at 1301.5 cm^{-1} exhibits the same annealing behavior with the 1843.1 cm^{-1} band, suggesting that the two absorptions are due to the different modes of the same molecule. The position of the 1301.5 cm^{-1} band indicates a La−H stretching vibration. Doping with CCl_4 has no effect on the two bands, which suggests that the product is neutral. The 1843.1 and 1301.5 cm^{-1} bands are therefore assigned to the N−N and La−H stretching vibrations of the neutral HLaNN molecule, respectively.

The present DFT calculations lend support for the assignment of HLaNN. The HLaNN molecule is predicted to have an $^3A''$ electronic ground state with a (core)$(a')^1(a'')^1(a')^0$ configuration and is 3.7 kcal/mol lower in energy than the $HLa(N_2)$ isomer with a (core)$(a'')^1(a'')^1(a'')^0$ configuration (Figure 5). NBO population analysis shows that there is about 0.011 e back donation from the HLa to N_2 subunit, similarly to that in HYNN, whereas the transfer from the N_2 subunit to the HLa moiety is about 0.027 e, much smaller than that in HYNN, accounting for the much lower N−N stretching vibrational frequency in HLaNN than in HYNN. The N−N and La−H stretching vibrations for HLaNN are calculated at 1834.5 and 1341.5 cm^{-1} (Tables 2 and 3), respectively, which supports the above assignment.

H_2LaNN. The absorption at 1854.1 cm^{-1} ($A = 0.026$) appears on annealing to 25 K and visibly increases on further annealing to 30 and 35 K (Table 1 and Figure 3). The 1854.1 cm^{-1} band shifts to 1793.3 cm^{-1} with $^{15}N_2$, exhibiting isotopic frequency ratio ($^{14}N/^{15}N = 1.0339$) characteristic of N−N stretching vibration. The mixed $^{14}N_2$ and $^{15}N_2$ isotopic spectra only provide the sum of pure isotopic bands (Figure 4), which indicates that only one N_2 subunit is involved in this mode. The position of 1854.1 cm^{-1} band indicates that an end-bonded N_2 subunit is involved. The absorption at 1276.7 cm^{-1} exhibits the same annealing behavior as that of the 1854.1 cm^{-1} band, suggesting that the two absorptions are due to the different modes of the same molecule. The position of the 1276.7 cm^{-1} band indicates a La−H stretching vibration. Doping with CCl_4 has no effect on the two bands, which suggests that the product is neutral. The 1854.1 and 1276.7 cm^{-1} bands are assigned to the N−N and La−H stretching vibrations of the neutral H_2LaNN molecule, respectively.

Similarly to H_2YNN, H_2LaNN is predicted to have a $^2A'$ ground state with C_s symmetry (Figure 5). The calculated N−N and La−H distances in H_2LaNN molecule are 1.149 and 2.116 Å, lengthened by 0.041 and 0.047 Å, respectively, compared with those in free N_2 and H_2La molecules. The N−N and antisymmetric La−H stretching vibrational frequency of H_2LaNN are calculated at 1943.9 and 1305.2 cm^{-1} (Tables 2 and 3). The calculated frequencies are harmonic ones, whereas the experimental frequencies are fundamental ones that are affected by the anharmonicity of the potential energy surface, which will result in some difference between the calculated values and experimental observations. DFT calculations also predict a symmetric La−H stretching vibrational frequency at 1340.7 cm^{-1}, which is unfortunately overlapped by other absorptions in the experiment.

Reaction Mechanism. On the basis of the behavior observed in the experiment, plausible reaction mechanisms can be proposed as follows. Laser ablation of an YH_2 target produces YH and YH_2 species, which are codeposited with N_2 to form the $HY(N_2)$, HYNN, and H_2YNN complexes on annealing to 25 K (Figure 1). These species increase on annealing, suggesting that the ground-state YH and YH_2 can react with N_2 to form the $HY(N_2)$, HYNN, and H_2YNN complexes spontaneously according to reactions 1−3, which are predicted to be exothermic by 10.5, 12.2, and 14.6 kcal/mol, respectively.

$$YH(^1\Sigma^+) + N_2 \rightarrow HY(N_2)(^3A) \qquad \Delta E = -10.5\text{kcal/mol} \quad (1)$$

$$YH(^1\Sigma^+) + N_2 \rightarrow HYNN(^3A'') \qquad \Delta E = -12.2\text{kcal/mol} \quad (2)$$

$$YH_2(^2A_1) + N_2 \rightarrow H_2YNN(^2A') \qquad \Delta E = -14.6\text{kcal/mol} \quad (3)$$

LaH, LaH_2, and LaH_3 are produced in the experiment of laser ablation of a LaH_x target. Laser-ablated LaH and LaH_2 are codeposited with dinitrogen molecules to form the HLaNN and H_2LaNN complexes on annealing to 25 K (Figure 3), which increase on further annealing, suggesting that the ground-state LaH and LaH_2 can react with dinitrogen molecules to form the HLaNN and H_2LaNN complexes spontaneously according to reactions 4 and 5, which are predicted to be exothermic by 19.8 and 17.5 kcal/mol, respectively. Although the reaction of LaH with N_2 to form the $HLa(N_2)$ molecule is exothermic (reaction 6), the $HLa(N_2)$ molecule is not observed in the present experiment. According to our DFT calculations, the end-on HYNN molecule is 1.7 kcal/mol lower in energy than the side-on $HY(N_2)$ isomer, and the HLaNN molecule is 3.5 kcal/mol lower in energy than the $HLa(N_2)$ isomer; the energy differences are small for both Y and La. A possible reason that $HY(N_2)$ molecule is detected whereas $HLa(N_2)$ molecule is not may come from the difference of barrier for the transformation from the end-on HMNN to the side-on $HM(N_2)$. The reaction energies of reactions 4 and 6 are predicted at the level of B3PW91/6-311++G(d, p)-SDD level, because the geometric optimization for the LaH molecule does not converge at the level of BP86/6-311++G(d, p)-SDD level.

$$LaH(^1\Sigma^+) + N_2 \rightarrow HLaNN(^3A'') \qquad \Delta E = -19.8\text{kcal/mol} \quad (4)$$

$$LaH_2(^2A_1) + N_2 \rightarrow H_2LaNN(^2A') \qquad \Delta E = -17.5\text{kcal/mol} \quad (5)$$

$$LaH(^1\Sigma^+) + N_2 \rightarrow HLa(N_2)(^3A'') \qquad \Delta E = -16.3\text{kcal/mol} \quad (6)$$

Conclusions

Reactions of laser-ablated yttrium and lanthanum hydrides with dinitrogen in excess argon have been studied by using infrared spectroscopy. On the basis of the isotopic shifts and splitting patterns, the molecules $HY(N_2)$, HYNN, H_2YNN, HLaNN, and H_2LaNN have been characterized. DFT calculations have been performed, which lend strong support to the experimental assignments of the infrared spectra. In addition, the plausible reaction mechanism for the formation of the products has been proposed.

Acknowledgment. The authors thank the reviewers for their valuable comments and suggestions. This work was supported by a Grant-in-Aid for Scientific Research (B) (Grant no. 17350012) from the Ministry of Education, Culture, Sports, Science and Technology (MEXT) of Japan. Y.-L.T. thanks JASSO and Kobe University for Honors Scholarship.

References and Notes

(1) Howard, J. B.; Rees, D. C. *Chem. Rev.* **1996**, *96*, 2965.
(2) Burgess, N. K.; Lowe, D. J. *Chem. Rev.* **1996**, *96*, 2983.
(3) Pool, J. A.; Lobkovsky, E.; Chirik, P. J. *Nature* **2004**, *427*, 527.
(4) Allen, A. D.; Senoff, C. V. *Chem. Commun.* **1965**, 621.
(5) Fryzuk, M. D.; Johnson, S. A. *Coord. Chem. Rev.* **2000**, *200*, 379.
(6) Hidai, M.; Mizobe, Y. *Chem. Rev.* **1995**, *95*, 1115.
(7) Richards, R. L. *Coord. Chem. Rev.* **1996**, *154*, 83.
(8) Siegbahn, P. E. M.; Blomberg, M. R. A. *Chem. Rev.* **2000**, *100*, 421.
(9) (a) Zhou, M. F.; Zhang, L.; Qin, Q. *J. Phys. Chem. A* **2001**, *105*, 6407. (b) Zhou, M. F.; Wang, G. J.; Zhao, Y. Y.; Chen, M. H.; Ding, C. F. *J. Phys. Chem. A* **2005**, *109*, 5079. (c) Zhou, M. F.; Jin, X.; Li, J. *Angew. Chem., Int. Ed.* **2007**, *46*, 2911.
(10) Chen, M. H.; Wang, G. J.; Zhou, M. F. *Chem. Phys. Lett.* **1998**, *409*, 70.
(11) (a) Chertihin, G. V.; Bare, W. D.; Andrews, L. *J. Phys. Chem. A* **1998**, *102*, 3697. (b) Teng, Y. L.; Xu, Q. *J. Phys. Chem. A*,in press. (c) Willson, S. P.; Andrews, L. *J. Phys. Chem. A* **1998**, *102*, 10238. (d) Chertihin, G.; Andrews, L.; Bauschlicher, C. W., Jr *J. Am. Chem. Soc.* **1998**, *120*, 3205. (e) Willson, S. P.; Andrews, L. *J. Phys. Chem. A* **1999**, *103*, 1311.
(12) (a) Schlapbach, L.; Zuttel, A. *Nature* **2001**, *414*, 353. (b) Percheron-Guégan, A.; Lartigue, C.; Achard, J. C. *J. Less-Common Met.* **1985**, *109*, 287. (c) Van Vucht, J. H. N.; Kuijpers, F. A.; Bruning, H. C. A. M. *Philips Res. Rep.* **1970**, *25*, 133.
(13) (a) Wang, X. F.; Chertihin, G. V.; Andrews, L. *J. Phys. Chem. A* **2002**, *106*, 9213. (b) Andrews, L. *Chem. Soc. Rev.* **2004**, *33*, 123.
(14) Teng, Y. L.; Xu, Q. *J. Phys. Chem. A* **2007**, *111*, 13380.
(15) (a) Zhou, M. F.; Andrews, L.; Bauschlicher, C. W., Jr *Chem. Rev.* **2001**, *101*, 1931. (b) Himmel, H. J.; Downs, A. J.; Greene, T. M. *Chem. Rev* **2002**, *102*, 4191, and references therein.
(16) (a) Burkholder, T. R.; Andrews, L. *J. Chem. Phys.* **1991**, *95*, 8697. (b) Zhou, M. F.; Tsumori, N.; Andrews, L.; Xu, Q. *J. Phys. Chem. A* **2003**, *107*, 2458. (c) Jiang, L.; Xu, Q. *J. Chem. Phys.* **2005**, *122*, 034505.
(17) Frisch, M. J.; Trucks, G. W.; Schlegel, H. B.; Scuseria, G. E.; Robb, M. A.; Cheeseman, J. R.; Montgomery, J. A., Jr.; Vreven, T.; Kudin, K. N.; Burant, J. C.; Millam, J. M.; Iyengar, S. S.; Tomasi, J.; Barone, V.; Mennucci, B.; Cossi, M.; Scalmani, G.; Rega, N.; Petersson, G. A.; Nakatsuji, H.; Hada, M.; Ehara, M.; Toyota, K.; Fukuda, R.; Hasegawa, J.; Ishida, M.; Nakajima, T.; Honda, Y.; Kitao, O.; Nakai, H.; Klene, M.; Li, X.; Knox, J. E.; Hratchian, H. P.; Cross, J. B.; Bakken, V.; Adamo, C.; Jaramillo, J.; Gomperts, R.; Stratmann, R. E.; Yazyev, O.; Austin, A. J.; Cammi, R.; Pomelli, C.; Ochterski, J. W.; Ayala, P. Y.; Morokuma, K.; Voth, G. A.; Salvador, P.; Dannenberg, J. J.; Zakrzewski, V. G.; Dapprich, S.; Daniels, A. D.; Strain, M. C.; Farkas, O.; Malick, D. K.; Rabuck, A. D.; Raghavachari, K.; Foresman, J. B.; Ortiz, J. V.; Cui, Q.; Baboul, A. G.; Clifford, S.; Cioslowski, J.; Stefanov, B. B.; Liu, G.; Liashenko, A.; Piskorz, P.; Komaromi, I.; Martin, R. L.; Fox, D. J.; Keith, T.; Al-Laham, M. A.; Peng, C. Y.; Nanayakkara, A.; Challacombe, M.; Gill, P. M. W.; Johnson, B.; Chen, W.; Wong, M. W.; Gonzalez, C.; Pople, J. A. *Gaussian 03*, revision B.04; Gaussian, Inc.: Wallingford, CT, 2004.
(18) (a) Becke, A. D. *Phys. Rev. A* **1988**, *38*, 3098. (b) Perdew, J. P. *Phys. Rev. B* **1986**, *33*, 8822. (c) Becke, A. D. *J. Chem. Phys.* **1993**, *98*, 5648. (d) Perdew, J. P.; Wang, Y. *Phys. Rev. B* **1992**, *45*, 13244.
(19) (a) Krishnan, R.; Binkley, J. S.; Seeger, R.; Pople, J. A. *J. Chem. Phys.* **1980**, *72*, 650. (b) Frisch, M. J.; Pople, J. A.; Binkley, J. S. *J. Chem. Phys.* **1984**, *80*, 3265.
(20) Dolg, M.; Stoll, H.; Preuss, H. *J. Chem. Phys.* **1989**, *90*, 1730.
(21) Souter, P. F.; Andrews, L. *J. Am. Chem. Soc.* **1997**, *119*, 7350.

JP8016024